Available online at www.sciencedirect.com
ScienceDirect
International Journal of Heat and Fluid Flow 28 (2007) 1507–1517
International Journal of HEAT AND FLUID FLOW
www.elsevier.com/locate/ijhff

The effect of two-way coupling and inter-particle collisions on turbulence modulation in a vertical channel flow

Hojjat Nasr, Goodarz Ahmadi *

Department of Mechanical and Aeronautical Engineering, Clarkson University, Potsdam, NY 13699-5725, United States

Received 14 December 2006; received in revised form 6 March 2007; accepted 8 March 2007
Available online 8 June 2007

Abstract

Turbulence modulation due to its interaction with dispersed solid particles in a downward fully developed channel flow was studied. The Eulerian framework was used for the gas-phase, whereas the Lagrangian approach was used for the particle-phase. The steady-state equations of conservation of mass and momentum were used for the gas-phase, and the effect of turbulence on the flow-field was included via the standard k–ε model. The particle equation of motion included the drag, the Saffman lift and the gravity forces. Turbulence dispersion effect on the particles was simulated as a continuous Gaussian random field. The effects of particles on the flow were modeled by appropriate source terms in the momentum, k and ε equations. Particle–particle collisions and particle–wall collisions were accounted for in these simulations. Gas-phase velocities and turbulence kinetic energy in the presence of 2–100% mass loadings of two particle classes (50 μm glass and 70 μm copper) were evaluated, and the results were compared with the available experimental data and earlier numerical results. The simulation results showed that when the inter-particle collisions were important and was included in the computational model, the fluid turbulence was attenuated. The level of turbulence attenuation increased with particle mass loading, particle Stokes number, and the distance from the wall. When the inter-particle collisions were negligible and/or was neglected in the model, the fluid turbulence was augmented for the range of particle sizes considered.

Keywords: Gas–solid flow; Turbulence modulation; Two-way coupling; Particle collision; Vertical channel

1. Introduction

There has been a continuing interest concerning turbulence modulation by presence of particles in recent decades. Despite many experimental and numerical simulation studies, the mechanism controlling the turbulence modulation process is not fully understood due to the large number of relevant parameters.

Available experimental data on particle-laden turbulent flows show that the addition of particles may increase or decrease the turbulence kinetic energy of the flow. Tsuji and Morikawa (1982) showed that small particles with diameter of about 200 μm attenuated the turbulence outside the viscous sublayer, while larger particles with diameter in the range of 3–4 mm lead to augmentation of turbulence fluctuations. Hetsroni (1989) and Gore and Crowe (1991) showed that, in general, small particles tend to damp the turbulence intensity while larger particles will increase the turbulence level. Gore and Crowe (1991) reported that the ratio of the particle diameter to a characteristic eddy diameter of the turbulence was the parameter that controlled whether fluid turbulence was attenuated or augmented. Hetsroni (1989), however, suggested that the particle Reynolds number was the key controlling parameter. Kulick et al. (1994) studied the turbulence modulation in a fully developed channel flow. In their study, particles were smaller than the Kolmogorov length scale of the flow and they showed that the fluid turbulence was attenuated by the addition of the particles and the level of attenuation increased with particle Stokes number, particle mass

* Corresponding author.
E-mail address: ahamdi@clarkson.edu (G. Ahmadi).

0142-727X/$ - see front matter © 2007 Published by Elsevier Inc.
doi:10.1016/j.ijheatfluidflow.2007.03.007

loading, and distance from the wall. Fessler and Eaton (1999) studied the turbulence modification by particles in a backward-facing step flow. They reported attenuation of the streamwise fluid turbulence in the extension region of the flow. No modification of the turbulence, however, was found in the separated shear layer or in the redevelopment region behind the step, although there were significant particle loadings in these regions. Elghobashi and Truesdell (1993) showed that several factors including gravitational field strength affected the turbulence decay rate. Yamamoto et al. (2001) studied the interaction between turbulence and solid particles in a fully developed channel flow using LES; they also considered the inter-particle collisions which were important for flows with high mass loading of particles.

Portela and Oliemans (2003) developed a code for the direct numerical simulation of particle-laden turbulent flows, using Eulerian–Lagrangian point-particle approach. When the two-way coupling was considered, they reported that the presence of particles led to large damping in the intensity of the streamwise vortices, without any significant change in their shape and their size. They also showed that this damping led to a weakening of the near wall streaky-pattern, and to a reduction in the accumulation of particles at the wall. Rashidi et al. (1990) performed an experimental study of particle–turbulence interactions near a wall, and they found that the near wall particle transport was mainly controlled by the turbulence burst phenomena. They also showed that presence of larger polystyrene particles (with diameter of 1100 μm) increased the number of wall ejections, and augmented the fluid turbulence, while smaller 120 μm polystyrene particles caused a decrease in the number of wall ejections, and attenuated the turbulence fluctuations. Yarin and Hetsroni (1994) studied the particle–turbulence interaction. They showed that finer particles damped the turbulence, while coarser particles enhanced it. They found that the level of turbulence modulation was affected by four parameters: the particle mass loading, the particle–fluid density ratio, the particle Reynolds number, and the ratio of the particle diameter to the characteristic eddy diameter.

Squires and Eaton (1991) simulated a homogeneous isotropic nondecaying turbulent flow-field by imposing an excitation at low wave numbers, and studied the effects of inertia on particle dispersion. They also used the DNS procedure to study the preferential microconcentration structure of particles as a function of Stokes number in turbulent near wall flows. Lain and Sommerfeld (2003) studied dispersed two-phase gas–solid flows using an Eulerian–Lagrangian approach including two-way coupling and analyzed turbulence modulation.

In this paper, the effects of inter-particle collisions on turbulence modulation caused by the presence of solid particles in a downward fully developed channel flow were studied. A hybrid (Eulerian–Lagrangian) model was used to solve the governing equations of particle and gas-phase. The effect of particles on the flow was considered by the appropriate source terms in the Eulerian governing equations of the gas-phase. The instantaneous turbulence fluctuation was simulated as a continuous Gaussian random field using the Kraichnan model. The drag, the Saffman lift and the gravity forces were included in the Lagrangian equation for particle motion. Particle–particle collisions as well as the particle–wall collisions were included in the simulations. Several computer simulations in the presence of two classes of particles (50 μm glass and 70 μm copper) were performed, and the results were compared with the experimental data of Kulick et al. (1994) and the LES results of Yamamoto et al. (2001).

2. Particle equation of motion

The particle motions are governed by Newton's second law. That is,

$$\frac{\mathrm{d}u_i^{\mathrm{p}}}{\mathrm{d}t} = \frac{3\nu C_{\mathrm{D}} Re_{\mathrm{p}}}{4d^2 S}(u_i - u_i^{\mathrm{p}}) + \frac{2Kd_{ij}}{Sd(d_{lk}d_{kl})^{\frac{1}{4}}}(u_j - u_j^{\mathrm{p}}) + g_i \qquad (1)$$

and

$$\frac{\mathrm{d}x_i}{\mathrm{d}t} = u_i^{\mathrm{p}} \qquad (2)$$

where $u_i = \overline{u_i} + u_i'$ is the instantaneous fluid velocity, $\overline{u_i}$ the mean velocity vector, u_i' the fluctuation velocity, u_i^{p} the particle velocity, x_i the particle position, t the time, d the particle diameter, S the ratio of particle density to fluid density, d_{ij} the deformation rate tensor, ν the kinematic viscosity, $K = 2.594$ the constant of Saffman's lift force, and g_i is the acceleration of gravity.

The first term on the right-hand side of Eq. (1) is the drag force. Drag force is always present and is generally the dominating force for particle motion in most regions of the flow. Here C_{D} is the drag coefficient, which varies with particles Reynolds number, Re_{p}. The drag coefficient for the solid particles is given as:

$$C_{\mathrm{D}} = \begin{cases} \frac{24}{Re_{\mathrm{p}}} & Re_{\mathrm{p}} < 1 \\ \frac{24}{Re_{\mathrm{p}}}\left(1 + 0.15Re_{\mathrm{p}}^{0.687}\right) & 1 < Re_{\mathrm{p}} < 1000 \\ 0.44 & Re_{\mathrm{p}} > 1000 \end{cases} \qquad (3)$$

Here the particle Reynolds number is defined as

$$Re_{\mathrm{p}} = \frac{d|u_i - u_i^{\mathrm{p}}|}{\nu} \qquad (4)$$

The second term on the right-hand side of Eq. (1) is the expression for the lift force provided by Saffman (1965, 1968) generalized to a three-dimensional shear field. (Note that the summation convention is suspended for the Saffman's lift force when $i = j$.)

2.1. Particle–wall collisions

Particle–wall collisions affect the nature of particle motion in the near wall region and also significantly affect the particle deposition rate on the wall. The effect of parti-

cle rebound from surface and its effect on particle deposition rate is included in the analysis. The wall surface potential arises due to the London–van der Waals force. At low impact velocities, small particles that strike a surface adhere to it. However, as the impact velocity increases, the particle may rebound from the surface. Bounce occurs when the kinetic energy of a particle is sufficiently large to overcome the wall potential of attractive forces. In this study, the wall surface potential is modeled as a boundary condition for the particle velocity. This approach originates from the observations that the effective length of the wall potential (of the order of ~Å) is much shorter than the fluid dynamical length scale (of the order of ~μm). Accordingly, the wall-normal velocity of the particle after the impact on the wall, $v^{\mathrm{p(after)}}$, is given as:

$$v^{\mathrm{p(after)}} = -\mathrm{sgn}(v^{\mathrm{p(before)}}) \times r\sqrt{(v^{\mathrm{p(before)}})^2 - V_{\mathrm{c}}^2} \tag{5}$$

where r is the coefficient of restitution, $v^{\mathrm{p(before)}}$ is the particle velocity normal to the wall before the impact. The critical velocity, V_{c}, is given by

$$V_{\mathrm{c}} = \sqrt{\frac{2\Phi(y_0)}{m}} \tag{6}$$

where $\Phi(y_0)$

$$\Phi(y_0) = \frac{Ad}{12y_0} \tag{7}$$

is the surface potential energy. According to Dahneke (1971), the minimum separation distance, y_0, is typically about 4 Å. In Eq. (7), A is the Hamaker constant (Hamaker, 1937). For most materials, A is of order of 10^{-20} J. The Hamaker constants for several materials were given by Dahneke (1972). When the wall-normal velocity of the particle is less or greater than V_{c}, respectively, capture or bouncing will occur.

2.2. Particle–particle collisions

The procedure for particle–particle collisions is the simple hard sphere model as described by Crowe et al. (1998) and Chen et al. (1998), among others. In this paper, the coefficient of restitution for the inter-particle collisions was taken to be 0.95. The collisions were assumed to be binary. Multiple collisions that were extremely rare for the range of concentration studied were neglected.

3. Gas-phase flow model

The governing equations for the motion of an incompressible fluid flow with a density ρ^{f}, and a kinematic viscosity υ, are the continuity and the Reynolds average Navier–Stokes equations. The effect of turbulence on the flow is modeled by the standard k–ε model. The corresponding governing equations for the carrier phase then are:

Continuity

$$\frac{\partial \overline{u_i}}{\partial x_i} = 0 \tag{8}$$

Momentum

$$\overline{u_j}\frac{\partial \overline{u_i}}{\partial x_j} = -\frac{1}{\rho^{\mathrm{f}}}\frac{\partial \overline{p}}{\partial x_i} + \nu\frac{\partial^2 \overline{u_i}}{\partial x_j \partial x_j} - \frac{\partial R_{ij}}{\partial x_j} + S_{u_i}^{\mathrm{p}} \tag{9}$$

Turbulence kinetic energy

$$\overline{u_j}\frac{\partial k}{\partial x_j} = \frac{\partial}{\partial x_j}\left[\left(\nu + \frac{\nu_{\mathrm{T}}}{\sigma^k}\right)\frac{\partial k}{\partial x_j}\right] - R_{ij}\frac{\partial \overline{u_i}}{\partial x_j} - \varepsilon + S_k^{\mathrm{P}} \tag{10}$$

Turbulence dissipation

$$\overline{u_j}\frac{\partial \varepsilon}{\partial x_j} = \frac{\partial}{\partial x_j}\left[\left(\nu + \frac{\nu_{\mathrm{T}}}{\sigma^{\varepsilon}}\right)\frac{\partial \varepsilon}{\partial x_j}\right] - C^{\varepsilon 1}\frac{\varepsilon}{k}R_{ij}\frac{\partial \overline{u_i}}{\partial x_j} - C^{\varepsilon 2}\frac{\varepsilon^2}{k} + S_{\varepsilon}^{\mathrm{P}} \tag{11}$$

where $\overline{p}$ is the mean pressure, R_{ij} the Reynolds stresses, $k = \frac{1}{2}\overline{u_i' u_i'}$ the turbulence kinetic energy, and ε is the turbulence dissipation energy. $S_{u_i}^{\mathrm{p}}$, S_k^{P}, and $S_{\varepsilon}^{\mathrm{P}}$ are the source terms due to presence of particles, respectively, in the mean flow, turbulence kinetic energy, and turbulence dissipation equations.

According to Boussinesq hypothesis, the Reynolds stress tensor can be written as:

$$R_{ij} = \frac{2}{3}k\delta_{ij} - 2\nu_{\mathrm{T}}\overline{d_{ij}} \tag{12}$$

where δ_{ij} is the Kroenecker Delta, ν_{T} the eddy viscosity, and $\overline{d_{ij}}$ is the deformation rate tensor defined as:

$$\nu_{\mathrm{T}} = C_{\mu}\frac{k^2}{\varepsilon}, \quad \overline{d_{ij}} = \frac{1}{2}(\overline{u_{i,j}} + \overline{u_{j,i}}) \tag{13}$$

The values of constants in Eqs. (10) and (11) are given as:

$$\sigma^k = 1, \quad \sigma^{\varepsilon} = 1.3, \quad C^{\varepsilon 1} = 1.44, \quad C^{\varepsilon 2} = 1.92 \tag{14}$$

3.1. Coupling between phases

The coupling between gas and disperse phases is implemented through momentum interaction term, $S_{u_i}^{\mathrm{p}}$ from the particle-phase to the gas-phase. $S_{u_i}^{\mathrm{p}}$ is the negative of the drag force acting on the particles exerted by the fluid in an Eulerian cell, and it is obtained by time and ensemble averaging for each control volume (Gouesbet and Berlemont, 1999; Lain and Sommerfeld, 2003). That is,

$$S_{u_i}^{\mathrm{p}} = -\frac{1}{\rho^{\mathrm{f}} V_{\mathrm{Cell}}}\sum_{k=1}^{N^{\mathrm{P}}} m_k N_k \Delta t_{\mathrm{L}} \times \sum_{n=1}^{N^{\mathrm{T}}}\left\{\frac{\left[(u_i^{\mathrm{p}})_k^{n+1} - (u_i^{\mathrm{p}})_k^{n}\right]}{\Delta t_{\mathrm{L}}} - g_i\left(1 - \frac{\rho_{\mathrm{f}}}{\rho_{\mathrm{p}}}\right)\right\} \tag{15}$$

In this expression, V_{Cell} is the volume of the computational cell which is given as:

$$V_{\mathrm{Cell}} = \mathrm{d}x \times \mathrm{d}y \times 1 \tag{16}$$

where dx and dy are the grid size in x and y directions. The sum over n indicates the number of time steps that one particle is tracked within the computational cell, N^{T} is the total number of time steps that a particle remains in the computational cell, and the sum over k is related to the number of particles passing through the cell, N^{P} is the number of particles which are tracked within the computational cell, $N_k\Delta t_{\mathrm{L}}$ is the number of real particles in one computational particle (in a computational Cell), and $m_{\mathrm{p}} = \rho^{\mathrm{P}}\pi\frac{d^3}{6}$ is the particle mass. In Eq. (15), Δt_{L} is the Lagrangian time step that is used in the solution of particle equation of motion.

The effect of particles on turbulence kinetic energy is expressed as an additional source term which is defined as (Lain and Sommerfeld, 2003):

$$S_k^{\mathrm{P}} = \overline{u_i^{\mathrm{p}} S_{u_i}^{\mathrm{P}}} - \overline{u_i}\,\overline{S_{u_i}^{\mathrm{P}}} \tag{17}$$

while the source term in ε-equation is modeled as:

$$S_\varepsilon^{\mathrm{P}} = C^{\varepsilon 3}\frac{\varepsilon}{k}S_k^{\mathrm{P}} \tag{18}$$

In this expression, it is assumed that $S_\varepsilon^{\mathrm{P}}$ is proportional to S_k^{P} and Lagrangian time scale of the turbulence $\left(\frac{\varepsilon}{k}\right)$. The constant value for $C^{\varepsilon 2}$ is not universal but depends on particle concentration and particle diameter. In this study, however, $C^{\varepsilon 2}$ is assumed to be 1.87 after Lain and Sommerfeld (2003).

3.2. Effect of turbulence on particles

Several models have been proposed to account for the effect of turbulence on the particle trajectories. The turbulence fluctuations are random functions of space and time. The Monte-Carlo velocity simulation techniques have been used as an economical method for generating time histories that have the random characters and statistical properties of turbulence. Kraichnan (1970) suggested a simple method for generating a Gaussian random field which resembles a pseudo-isotropic turbulence. Accordingly, the scaled instantaneous fluctuating velocity is given as

$$\vec{u}^{I*}(x^*,t^*) = \sqrt{\frac{2}{N}}\left\{\sum_{n=1}^{N}\vec{u_1}(\vec{k_n})\cos(\vec{k_n}\cdot\vec{x^*}+\omega_n t^*) + \sum_{n=1}^{N}\vec{u_2}(\vec{k_n})\sin(\vec{k_n}\cdot\vec{x^*}+\omega_n t^*)\right\} \tag{19}$$

In this equation

$$\vec{u_1}(\vec{k_n}) = \vec{\zeta}\times\vec{k_n}, \quad \vec{u_2}(\vec{k_n}) = \vec{\xi}\times\vec{k_n} \tag{20}$$

$$\vec{k_n}\cdot\vec{u_1}(\vec{k_n}) = \vec{k_n}\cdot\vec{u_2}(\vec{k_n}) = 0 \tag{21}$$

Eq. (21) ensures the incompressibility condition. The components of vectors $\vec{\zeta}_n$ and $\vec{\xi}_n$ and the frequencies ω_n are picked independently from Gaussian distribution with a standard deviation of unity. Each component of $\vec{k_n}$ is a Gaussian random number with a standard deviation of 1/2. Here, N is the number of terms in the series.

In Eq. (19), the dimensionless quantities are defined as

$$x^* = \frac{x}{l_0}, \quad t^* = \frac{t}{t_0}, \quad u_i^{I*} = \frac{u_i^{I\prime}}{u_0^*} \tag{22}$$

where l_0, t_0 and u_0^* are the length, time and the velocity scales of turbulence and $u_i^{I\prime}$ is the fluctuation fluid velocity. For this pseudo-turbulent velocity field the energy spectrum $E(k)$ is given by

$$E(k) = 16\left(\frac{2}{\pi}\right)^{\frac{1}{2}}k^4\,\mathrm{e}^{-2k^2} \tag{23}$$

where k is the wave number.

The instantaneous turbulent fluctuating velocity vector is then given by

$$u_i' = u_i^{I\prime}e_i(y), \quad \text{no sum on } i \tag{24}$$

where $e_i(y)$ are the shape functions for the axial, vertical, and transverse RMS velocities. (Here 1, 2, and 3 stand for x-, y-, and z-directions, respectively.) Estimates for the length and time scales of turbulent flows were provided by Davies (1972). Accordingly,

$$l_0 = 0.1h(2Re)^{-\frac{1}{8}}, \quad t_0 = \frac{l_0}{u^*} = \frac{2h}{20u^*(2Re)^{\frac{1}{8}}} = \frac{h}{2V} \tag{25}$$

Eqs. (19) and (24), with $N = 100$, together with (25) were used for simulating the fluctuation components of turbulent velocity in a channel. It should be emphasized that the Kraichnan (1970) model was developed for simulating isotropic flows. Here with use of scaling factors given by Eq. (24) and the length and time scales given by (25), an anisotropic turbulence fluctuation near a wall can be simulated. The simulated flows lead to proper variation of mean-square fluctuations and appropriate turbulence diffusivity. However, it is still a random Gaussian field and does not have the proper spectral energy distribution of turbulence.

4. Eulerian-to-Lagrangian and Lagrangian-to-Eulerian grid-mapping

Gas-phase velocities, turbulence kinetic energy and turbulence energy dissipation from the Eulerian approach are evaluated at the face and center of the staggered grids. However, for evaluating the forces acting on the particles, the gas velocities at the locations of particles must be evaluated by certain interpolation techniques. Similarly, the forces acting from the particles on the gas-phase are exerted at the particle position. To account for two-way interactions in the computation of the gas-phase motion, an interpolation technique is needed to transfer these forces onto the staggered computational grids. Here, an area-averaged interpolation scheme for Eulerian-to-Lagrangian grid-mapping is used. i.e.,

$$\phi_{\mathrm{L}} = \frac{1}{\mathrm{d}x\mathrm{d}y}(\phi_{\mathrm{E}1}A_3 + \phi_{\mathrm{E}2}A_4 + \phi_{\mathrm{E}3}A_1 + \phi_{\mathrm{E}4}A_2) \tag{26}$$

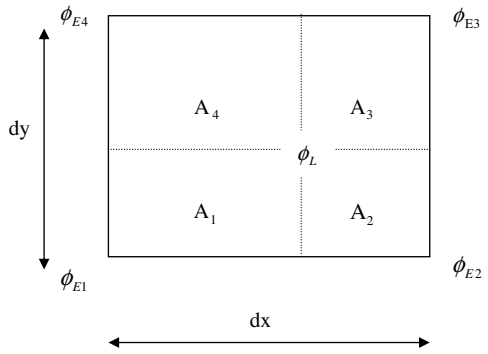

Fig. 1. Schematic of Eulerian-to-Lagrangian interpolation scheme.

where ϕ_L is the estimated local properties (gas-velocity) for the Lagrangian approach, ϕ_{E1}–ϕ_{E4} are properties (gas velocities) at the grid nodes of the Eulerian frame, and A_1–A_4 are areas of cell fractions shown in Fig. 1.

The interpolation scheme used for Lagrangian-to-Eulerian grid-mapping reads

$$\phi_{E1} = \frac{\phi_L A_3}{dxdy} \quad \phi_{E2} = \frac{\phi_L A_4}{dxdy}$$
$$\phi_{E3} = \frac{\phi_L A_1}{dxdy} \quad \phi_{E4} = \frac{\phi_L A_2}{dxdy} \tag{27}$$

where in this case, ϕ_L is the force acting on the particles in the Lagrangian frame and ϕ_{E1}–ϕ_{E4} are the transmitted forces to the Eulerian grid nodes.

5. Numerical procedure

In this study, an Eulerian–Lagrangian computation model for analyzing turbulent gas–solid flow in a two dimensional channel was developed. The new code (STARPIC-TP) is based on STARPIC computer code developed by Lilley and Rhode (1982) extended to two-phase flows. The gas-phase is the continuous-phase and the particles are treated as the dispersed phase. The code solves the incompressible RANS and the standard k–ε equations for the gas-phase in gas–solid flows with the coupling effect of particle being included as sources that are evaluated by a cell-averaged approach. A finite-difference method was used to discretize the gas-phase equations on a structured, staggered grid. The particle motion is simulated by the Lagrangian trajectory analysis procedure. Two-way coupling between the gas-phase and the particles is accounted for. The particle-phase equations are solved using the Runge–Kutta-4 method. When particles hit the wall or when two particles collide, the final coordinates and velocities of the particles are modified to account for the particle–wall and particle–particle collisions. An iterative procedure between Eulerian mean flow calculation and the Lagrangian particle tracking was used to account for the two-way coupling as described by the following procedure:

(1) A fully developed velocity profile is used as an inlet boundary condition for the channel flow.
(2) The code solves the gas-velocity field first (gas-phase solver).
(3) Due to the importance of the inter-particle collisions on the results, this step is done in the following two sub-steps:
   (a) When the new values for the velocity are obtained, particles which are uniformly distributed in the channel with the initial velocity equal to the local gas-velocity are tracked in the known gas-velocity for a long time (about 20 times the particle relaxation time) considering the inter-particle collisions. In this sub-step, the source terms are not evaluated and particles are tracked until the particle mean velocity profile reaches a statistically stationary state then the second sub-step is followed.
   (b) Particles are tracked in the channel, and the values for the source terms are evaluated. It is important to note that in this sub-step, each particle is tracked until it passes the entire length of the channel just once. For example, when the initial location of a particle is in the middle of the channel, that particle is tracked until it goes out of the channel, and again it is tracked for the remained path, and when it reaches its initial x-coordinate, it is no longer tracked. (Periodic boundary condition is set at inlet and outlet for particles.)
(4) For this step the gas governing equations are solved by the addition of source terms due to the presence of particles in the flow (coupling between the continuous-phase and the particles).
(5) After obtaining the converged solution for the gas-phase field, all the particles are tracked again in order to identify their corrected positions and the improved interaction source terms.
(6) This iterative procedure is repeated until convergence is achieved.

6. Results and discussions

In this section, the simulation results for fluid and particle velocities, turbulence kinetic energy, and turbulence dissipation for different particle mass loadings are presented. The Simulations were performed for a 2D downward fully developed channel, which is 4 cm wide and 1.0 m long. (For the test of accuracy, simulations were also performed for a 2.0 m long channel, and no noticeable difference in the results was seen.) All simulations were performed for a centerline air velocity of 10.5 m/s, corresponding to a Reynolds number of 13,800 based on the channel half-width, which are identical to the experimental conditions of Kulick et al. (1994). A temperature of 288 K, $\mu = 1.85 \times 10^{-5}$ N s/m^2, and $\rho = 1.225$ kg/m^3 for air are

assumed. Wall units are used for comparison with the experimental data with

$$y^+ = \frac{yu^*}{\nu}, \quad u^+ = \frac{u}{u^*} \tag{28}$$

where ν is the kinematic viscosity and u^* is the friction velocity. Kulick et al. (1994) reported a value of $u^* = 0.49$ m/s for the friction velocity in their experiments. Their experiments were performed for different concentration of 50 μm glass particles with a density of 2500 kg/m^3 and 70 μm copper particles with a density of 8800 kg/m^3.

In the simulation a fully developed profile corresponding to the experimental gas flow rate was imposed as an inlet boundary condition. The simulation results for different particle mass loadings are presented in this section and are compared with the experimental data of Kulick et al. (1994) and the LES simulation results of Yamamoto et al. (2001). Initially, particles are distributed uniformly in the computational domain and are assumed to have the same velocity as the local gas flow. When a particle hits the wall, the wall collision model provides the new particle velocity and the new particle position after rebound. In all simulations the coefficient of restitution was set equal to 0.95. In order to study the effect of inter-particle collisions on the flow, all simulations were repeated for the cases that the inter-particle collisions were included or ignored.

6.1. Mean fluid velocity

Figs. 2 and 3, respectively, compare the predicted streamwise fluid velocity in the presence of different mass loadings of 50 μm glass and 70 μm copper particles with the experimental data of Kulick et al. (1994) and the LES simulations of Yamamoto et al. (2001). These figures show

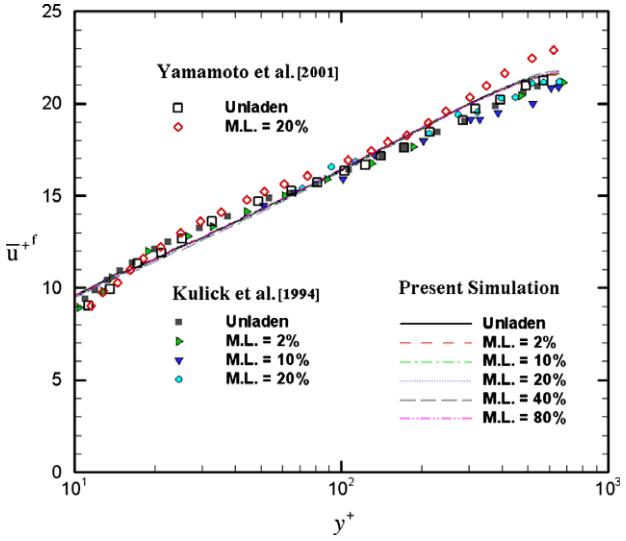

Fig. 2. Comparison of the present simulations results for gas-phase mean streamwise velocity profile in the presence of 50 μm glass particles with the experimental data of Kulick et al. (1994) and the LES of Yamamoto et al. (2001).

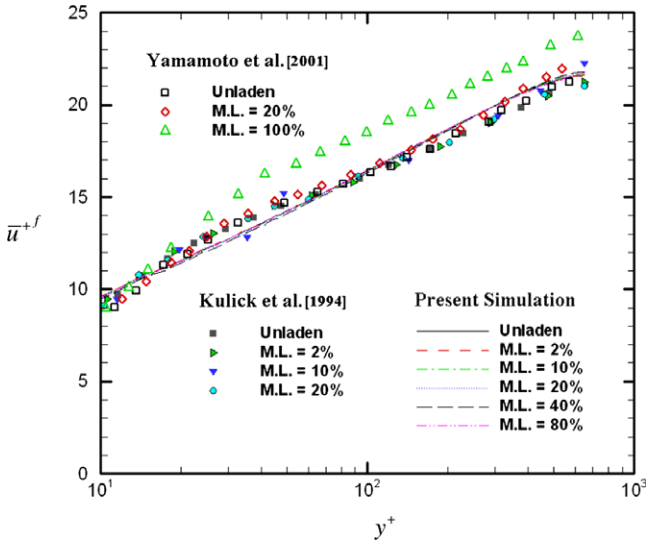

Fig. 3. Comparison of the present simulations results for gas-phase mean streamwise velocity profile in the presence of 70 μm glass particles with the experimental data of Kulick et al. (1994) and the LES of Yamamoto et al. (2001).

no apparent modification of the streamwise fluid velocity due to the presence of particles. As noted before, the gas flow rate was kept constant in the experimental study of Kulick et al. (1994) and the present simulation for different mass loadings. Therefore, no significant change in the mean fluid velocity is observed. The present simulation results for the streamwise fluid velocity are in good agreement with the experimental data of Kulick et al. (1994).

The LES simulation of Yamamoto et al. (2001) predicted that the mean streamwise fluid velocity remains unchanged up to a mass loading of M.L. = 20%. They also found that, in the case of very high mass loading of particles (M.L. = 100%) the mean fluid velocity changes and shifts upward in the logarithmic region as shown in Figs. 2 and 3. It should be pointed out that Yamamoto et al. (2001) assumed a constant pressure gradient, while in the experimental work and the present simulation the gas flow rate was constant. The addition of particles in a downward gas flow increases the mean gas-velocity under a constant pressure gradient, which is seen in the simulation of Yamamoto et al. (2001).

6.2. Mean particle velocity

Figs. 4 and 5 show the mean particle velocity profiles of 50 μm glass particles with $\tau_p = 0.02$ s and 70 μm copper particles with $\tau_p = 0.1$ s for different mass loadings in the range of 2–100%. Here τ_p is the particle relaxation time defined as:

$$\tau_p = \frac{d^2 S}{18\nu} \tag{29}$$

It is seen that the mean velocity profile of the particles is flatter than that of the flow, and as mass loading and par-

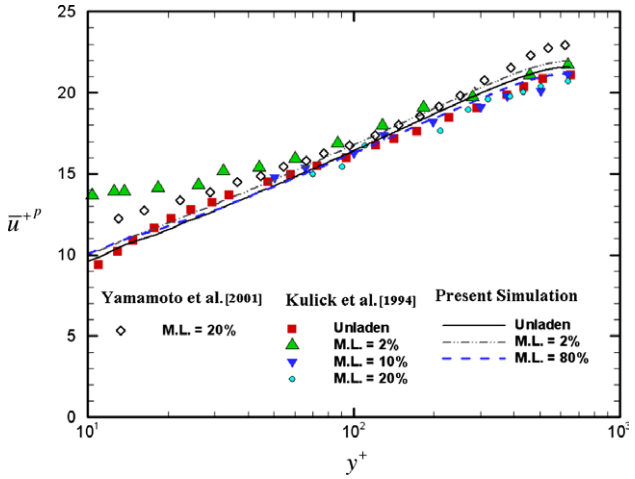

Fig. 4. Comparison of the present simulations results for 50 μm glass particle streamwise mean velocity profile with the experimental data of Kulick et al. (1994) and the LES of Yamamoto et al. (2001).

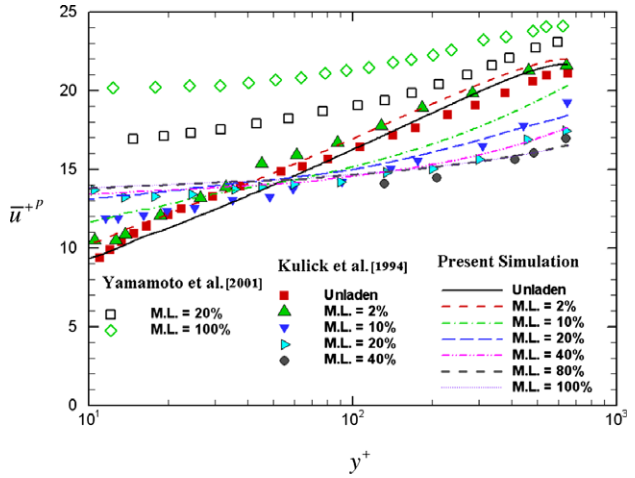

Fig. 5. Comparison of the present simulations results for 70 μm copper particle streamwise mean velocity profile with the experimental data of Kulick et al. (1994) and the LES of Yamamoto et al. (2001).

ticle relaxation time increase, particle velocity profile becomes more flat. The 50 μm glass particles have nearly the same velocity profile as the local gas flow in the core and somewhat higher near the wall. Close examination of the simulation results shows that while there are many collisions between 50 μm glass particles, but because the relaxation of these particles is low (0.02 s), the glass particles follow the flow. When heavier 70 μm copper particles collide, a large fraction of streamwise particle velocity is converted to the normal velocity, which leads to the so-called transverse mixing. As a result, the particle velocity profile becomes significantly more flat. It is important to note that although the number of collisions for 50 μm glass particles is higher than that for 70 μm copper particles, the motion of 70 μm copper particles is significantly influenced by the inter-particle collisions. The 50 μm glass particles respond to the flow much faster than 70 μm copper particles after collision due to their different particle relaxation times.

Figs. 4 and 5 show that the simulated mean particle velocities are in favorable agreement with the experimental data of Kulick et al. (1994). The LES simulation results of Yamamoto et al. (2001) for mean particle velocities, shown in Figs. 4 and 5, appear to deviate from the experimental data. Fig. 5 shows that the LES simulations of Yamamoto et al. (2001) for the 70 μm copper particles predict that the particles move faster than the flow both in the core and in the wall region. The experimental data of Kulick et al. (1994) shows that the particles lag the flow in the core due to transverse mixing. One possible explanation is that the computation time of the LES simulation might not have been sufficient to produce statistically accurate results for the steady mean particle velocity.

In the present study, particles are allowed to collide for a long time and when the mean particle velocity reaches a steady-state solution, the source terms due to the presence of particles are evaluated. This could explain in part the better agreement obtained in the present simulation.

The particle concentration was also evaluated, which showed a roughly uniform variation across the channel with a slight increasing trend toward the wall. The roughly uniform variation is perhaps due to the particle–particle and particle–wall collisions as suggested by Kulick et al. (1994).

6.3. Turbulence modification

The effects of particles on the turbulence kinetic energy of the gas flow for different particle mass loadings with and without inter-particle collisions are shown in Figs. 6 and 7. For both 50 μm glass and 70 μm copper particles when the inter-particle collisions in the simulation are turned off,

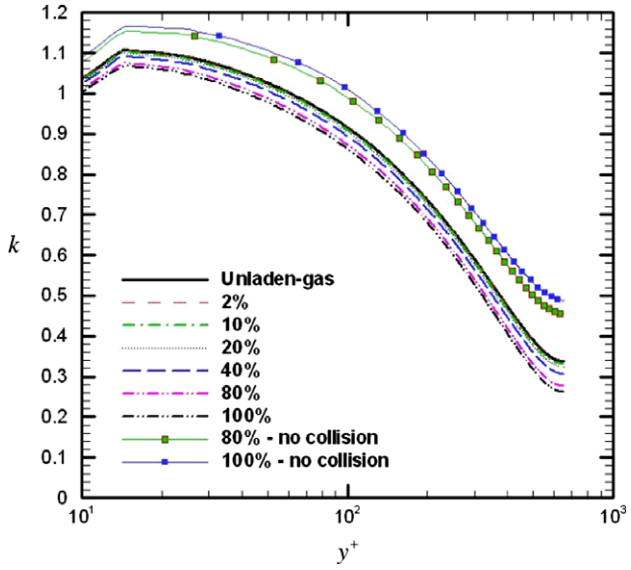

Fig. 6. Present simulated results for turbulence kinetic energy in the presence of 50 μm glass particles at different mass loadings.

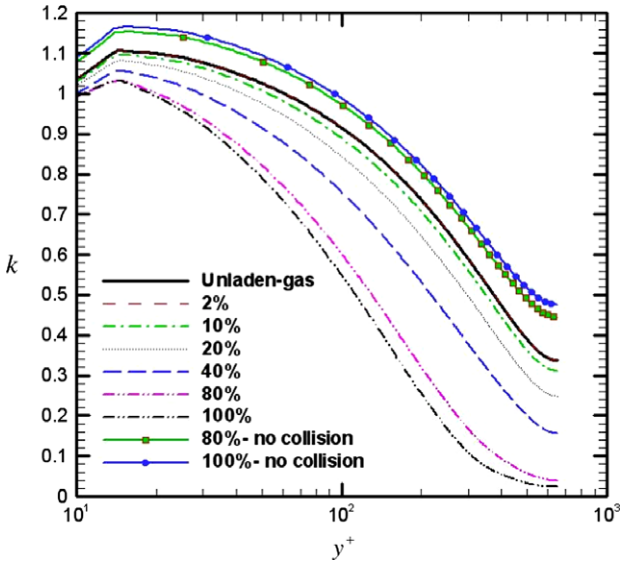

Fig. 7. Present simulated results for turbulence kinetic energy in the presence of 70 μm copper particles at different mass loadings.

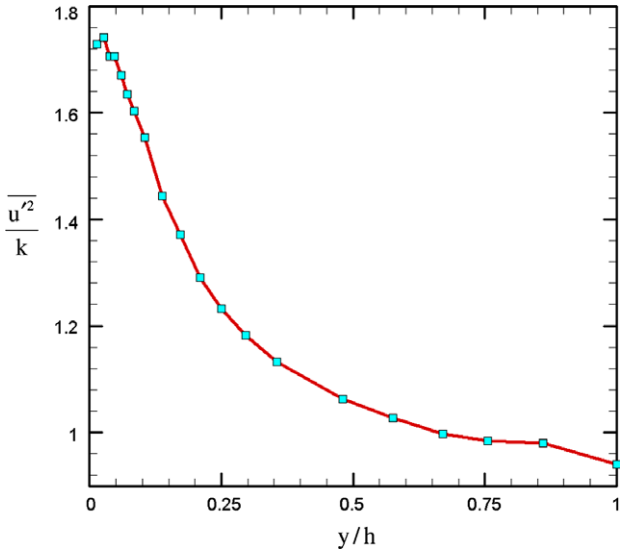

Fig. 8. The ratio of the streamwise turbulence fluctuation energy to the turbulence kinetic energy based on the experimental data of Kreplin and Eckelmann (1979).

augmentation in turbulence kinetic energy occurs. As mass loading increases, the level of augmentation increases. When the inter-particle collisions are taken into account, the simulation predicts attenuation in turbulence kinetic energy. The level of attenuation for copper particles is higher than that for the glass particles, and as mass loading increases the attenuation of turbulence increases. When the inter-particle collisions are ignored in the simulation, particles move faster than the flow due to gravitational sedimentation, and they tend to make the gas flow move faster. However, because the gas flow rate is forced to be constant, and the exerted drag forces of the particles are uniformly distributed in the channel, the gas-velocity profile remains roughly unchanged. As a result, the pressure drop decreases and the Reynolds stresses (turbulence kinetic energy) increase.

When the effect of inter-particle collisions are included, transverse mixing occurs and particles lag the flow in the core. As a result, particles exert a drag force on the gas-phase but due to the constant gas flow rate, the pressure drop increases and Reynolds stresses decrease. From the presented results, it is concluded that inter-particle collisions play a crucial role in turbulence attenuation process.

Comparison of the present simulation results for the streamwise turbulence intensity profiles with the experimental data of Kulick et al. (1994) and the LES simulations of Yamamoto et al. (2001) are performed in Figs. 9–11. To calculate the streamwise turbulent intensity, the ratio of $\overline{u'^2}/k$ was evaluated from the experimental data of Kreplin and Eckelmann (1979) and was used to estimate $\overline{u'^2}$ from the present simulation results for k. Fig. 8 shows the variation of $\overline{u'^2}/k$ across the duct. It is seen that the ratio has a peak of about 1.75 very close to the wall and decreases to about 0.7 at the duct centerline. It should be emphasized that the use of Eq. (12) for evaluating $\overline{u'^2}$ from the value of k will not lead to proper variation of streamwise fluctuation velocity since this equation incorrectly assumes isotropy of turbulence fluctuation.

Figs. 9–11 show that the predicted levels of attenuation of the present simulation are in agreement with the experimental data of Kulick et al. (1994). While the LES simulations of Yamamoto et al. (2001) captures the trend of the variation of the experimental data, the magnitude of the turbulence intensity is overestimated near the wall. It is observed that the LES simulation of Yamamoto et al. (2001) for the streamwise turbulence intensity at 20% mass loading does not show a noticeable level of attenuation, but the experimental data of Kulick et al. (1994) and the present simulation results lead to an attenuation of streamwise turbulence intensity by about 40%. This discrepancy of

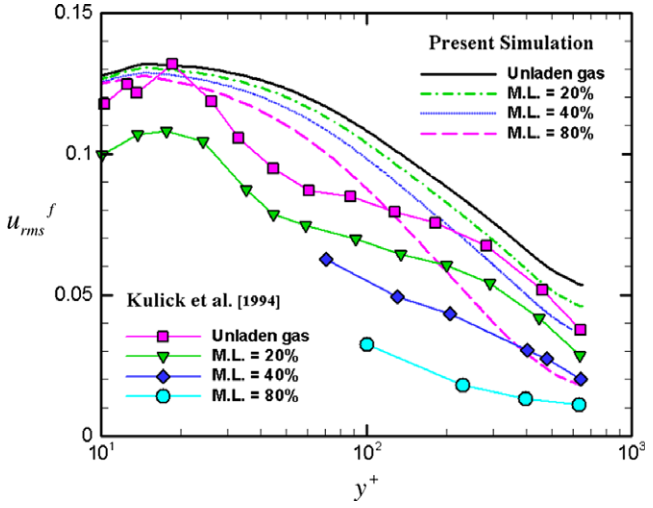

Fig. 9. Comparison of the present simulation results for gas streamwise turbulent intensity in the presence of 70 μm copper particles with the experimental data of Kulick et al. (1994).

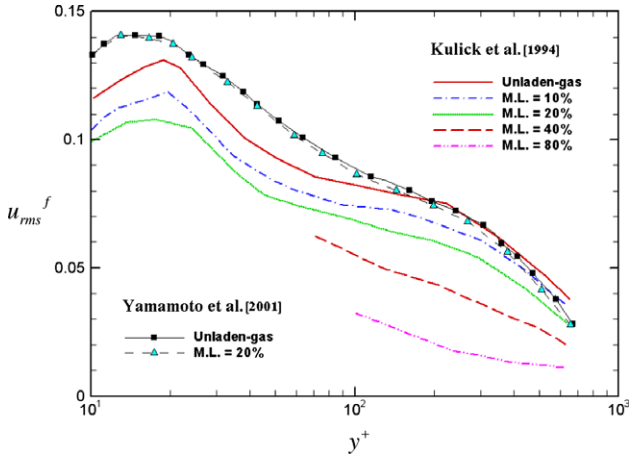

Fig. 10. Comparison of the experimental data of Kulick et al. (1994) with the LES simulations of Yamamoto et al. (2001) for gas streamwise turbulent intensity in the presence 70 μm copper particles.

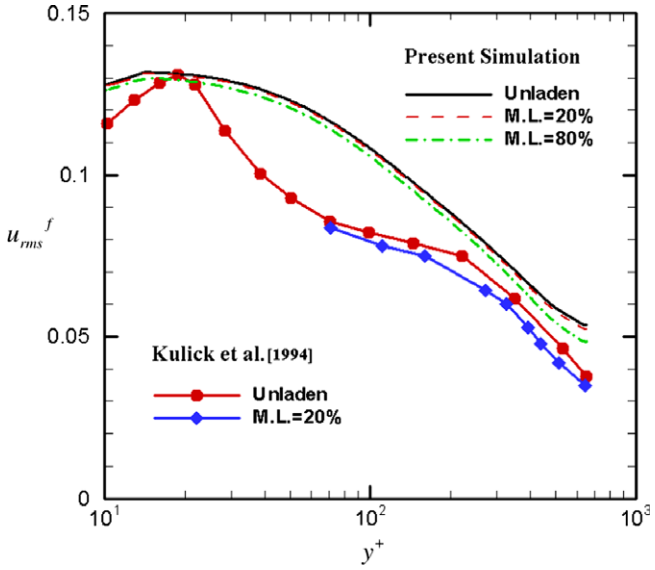

Fig. 11. Comparison of the present simulation results for gas streamwise turbulent intensity in the presence of 50 μm glass particles with the experimental data of Kulick et al. (1994).

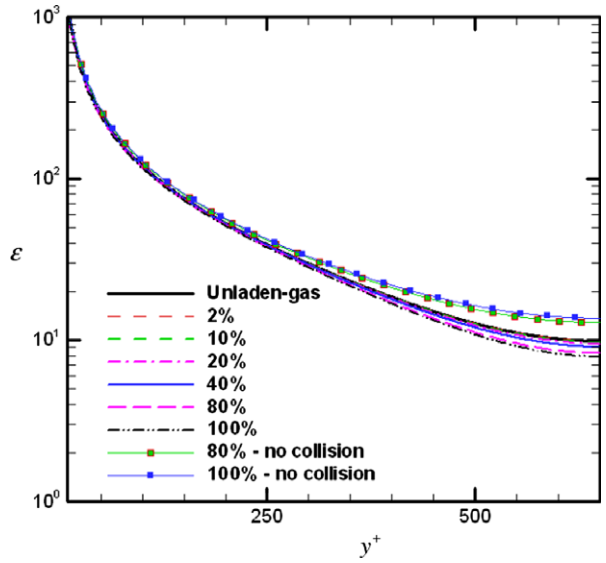

Fig. 12. Present simulation results for turbulence dissipation rate in the presence of 50 μm glass particles.

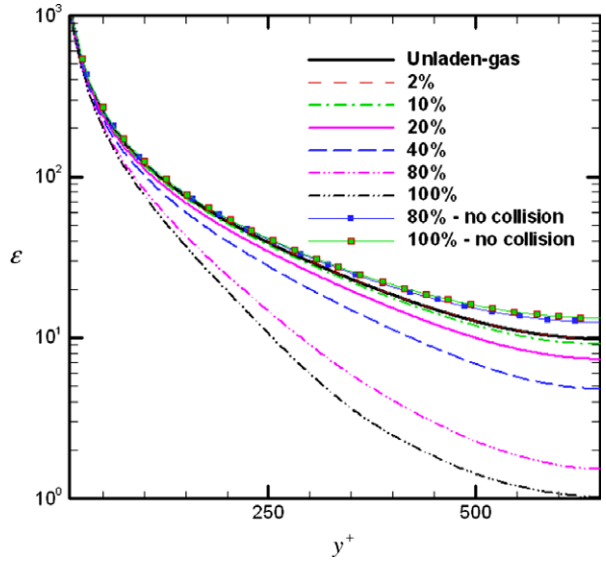

Fig. 13. Present simulation results for turbulence dissipation rate in the presence of 70 μm copper particles.

LES results could be due to prediction of mean particle velocity which is higher than the mean fluid velocity as is seen in Fig. 5.

Fig. 11 compares the present simulation for the streamwise turbulence intensity in the presence of 50 μm glass beads with the experimental data of Kulick et al. (1994). It is seen that turbulence attenuation due to the presence of the 50 μm glass beads is lower than that for 70 μm copper particles.

Figs. 12 and 13, respectively, show the effects of particles on the turbulence dissipation rate for 50 μm glass and 70 μm copper particles. It is seen that when the inter-particle collisions are not considered, the simulation predicts an increase of the turbulence dissipation rate. As mass loading increases, the magnitude of turbulence dissipation rate also increases. When the inter-particle collisions are included in the analysis, the simulation leads to a decrease in turbulence dissipation rate and the level of attenuation increases with an increase in mass loading, particle relaxation time, and distance from the wall.

Kulick et al. (1994) measured the turbulence kinetic energy and turbulence dissipation at the center of the channel in presence of different mass loadings of 70 μm copper particles. Their experimental data for k/k^{Unladen} and $\varepsilon/\varepsilon^{\text{Unladen}}$ are reproduced in Fig. 14. Here k^{Unladen} and $\varepsilon^{\text{Unladen}}$ are unladen values at the channel centerline. The present simulation results in the presence and absence of particle collisions are shown in this figure for comparison. It is observed that when the inter-particle collisions are

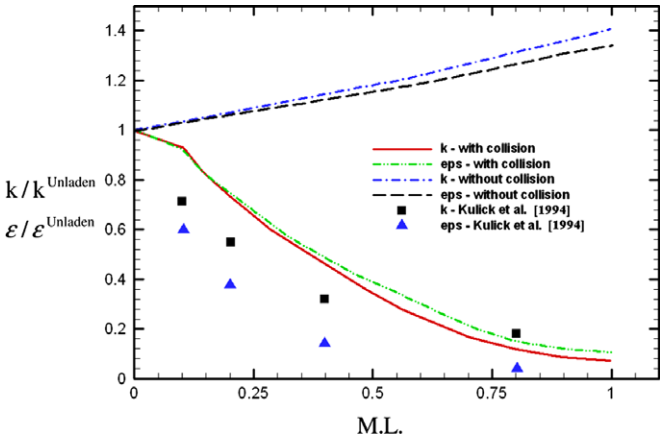

Fig. 14. Modulation of turbulence kinetic energy and turbulence dissipation rate with mass loading for 70 μm copper particles at the center of the channel.

included in the simulation, in agreement with the experimental data of Kulick et al. (1994), both turbulence kinetic energy and turbulence dissipation rate are attenuated. The level of attenuation increases as particle mass loading increases. The predicted amount of attenuation, however, is lower than that observed in the experiment.

When the effect of particle collisions are neglected in the simulation, the trend of the predicted behavior is opposite to the experimental data and suggest augmentation of turbulence.

7. Conclusions

The interaction between solid particles and gas-phase in a downward fully developed channel flow was investigated. A hybrid (Eulerian–Lagrangian) model was used to solve the coupled governing equations of gas-particle flows. The effect of particles on the flow was considered by inclusion of appropriate source terms in the Eulerian governing equations of the gas-phase. The instantaneous turbulence fluctuation was simulated as a continuous Gaussian random field using the Kraichnan model. The drag, the Saffman lift and the gravity forces were accounted for in the Lagrangian equation of particle motion. Particle–particle collisions as well as the particle–wall collisions were included in the simulation. Several simulations in the presence of two classes of particles, 50 μm glass and 70 μm copper particles, were performed, and the results were compared with the experimental data of Kulick et al. (1994) and the LES simulation of Yamamoto et al. (2001). On the basis of the results presented, the following conclusions may be drawn:

(1) Computation simulation provides a viable method for studying turbulence modulation process.
(2) Under fixed flow rate condition, no apparent modification of the mean flow velocity profile due to the presence of particles is observed, which is in agreement with the experimental data of Kulick et al. (1994).
(3) When particle–particle collisions are included in the simulation, the predicted mean particle velocity profile becomes flatter than the mean fluid velocity profile due to the transverse mixing phenomenon.
(4) The motion of 70 μm copper particles is significantly affected by the inter-particle collisions, while for 50 μm glass particles the inter-particle collision effect is less important.
(5) Due to the condition of constant gas flow rate in this study, the addition of particles changes both the pressure gradient and the Reynolds stresses to balance the addition of particle drag force on the flow.
(6) It is observed that when the inter-particle collisions are included in the simulation, turbulence attenuation occurs. This is in agreement with the experimental data of Kulick et al. (1994). Therefore, for studying turbulence modulation due to the presence of particles, inter-particle collisions have to be included in the analysis.
(7) The level of turbulence attenuation for 70 μm copper particles is higher than that for 50 μm glass particles. It is conjectured that this is because of the differences in the mean particle velocities. The mean streamwise velocity of copper particles is smaller than that of glass particles due to the high level of transverse mixing. Therefore, the copper particles exert a larger drag force on the flow when compared with the glass particles. As a result, the presence of copper particles exerts a larger damping force on the flow compared to the glass beads.

The present approximate method that uses the k–ε turbulence model was found to provide a useful tool for studying turbulence modulation in a downward channel flow. There are many additional important effects that were not addressed in the present study. For example, the effect of direction of gravity, parametric study of turbulence modulation for a large range of particle concentrations and material properties are left for the future studies.

Acknowledgements

The financial support of the Environmental Protection Agency (EPA) and the NYSTAR Center of Excellence is gratefully acknowledged.

References

Chen, M., Kontomaris, K., McLaughlin, J.B., 1998. Direct numerical simulation of droplet collisions in a turbulent channel flow. Part I: Collision algorithm. Int. J. Multiphase Flow 24, 1079–1103.
Crowe, C., Sommerfeld, M., Tsuji, Y., 1998. Multiphase Flows with Droplets and Particles. CRC Press, Boca Raton, FL.
Dahneke, B., 1971. The capture of aerosol particles by surfaces. J. Colloid Interf. Sci. 37, 342–353.
Dahneke, B., 1972. The influence of flattening on the adhesion of particles. J. Colloid Interf. Sci. 40, 1–13.
Davies, J.T., 1972. Turbulence phenomena. Academic Press, New York.

Elghobashi, S.E., Truesdell, G.C., 1993. On the two-way interaction between homogeneous turbulence and dispersed solid particles. I: Turbulence modification. Phys. Fluids A 5, 1790–1801.

Fessler, J.R., Eaton, J.K., 1999. Turbulence modification by particles in a backward facing step. J. Fluid Mech. 394, 97–117.

Gore, R.A., Crowe, C.T., 1991. Modulation of turbulence by a dispersed phase. Trans. ASME I: J. Fluid Eng. 113, 304–307.

Gouesbet, G., Berlemont, A., 1999. Eulerian and Lagrangian approaches for predicting the behavior of discrete particles in turbulent flows. Prog. Energy Combust. Sci. 25, 133–159.

Hamaker, H.C., 1937. The London–van der Waals attraction between spherical particles. Physica IV (10), 1058–1072.

Hetsroni, G., 1989. Particles–turbulence interaction. Int. J. Multiphase Flow 15, 735–746.

Kraichnan, R.H., 1970. Diffusion by random velocity field. Phys. Fluid 11, 43–62.

Kreplin, H., Eckelmann, H., 1979. Behaviour of the three fluctuating velocity components in the wall region of a turbulent channel flow. Phys. Fluids 22, 1233.

Kulick, J.D., Fessler, J.R., Eaton, J.K., 1994. Particle response and turbulence modification in fully developed channel flow. J. Fluid Mech. 277, 109–134.

Lain, S., Sommerfeld, M., 2003. Turbulence modulation in dispersed two-phase flow laden with solids from a Lagrangian perspective. Int. J. Heat Fluid Flow 24, 616–625.

Lilley, D.G., Rhode, D.L., 1982. A computer code for swirling turbulent axisymmetric recirculating flows in practical isothermal combustor geometries. NASA Contractor Report 3442.

Portela, L.M., Oliemans, R.V.A., 2003. Eulerian–Lagrangian DNS/LES of particle–turbulence interactions in wall-bounded flows. Int. J. Numer. Meth. Fluids 43, 1045–1065.

Rashidi, M., Hetsroni, G., Banerjee, S., 1990. Particle–turbulence interaction in a boundary layer. Int. J. Multiphase Flow 16, 935–949.

Squires, K.D., Eaton, J.K., 1991. Measurements of particle dispersion obtained from direct numerical simulations of isotropic turbulence. J. Fluid Mech. 226, 1–35.

Saffman, P.G., 1965. The lift force on a small sphere in a slow shear flow. J. Fluid Mech. 22, 385–400.

Saffman, P.G., 1968. Corrigenda. J. Fluid Mech. 31, 624.

Tsuji, Y., Morikawa, Y., 1982. LDV measurements of an air–solid two-phase flow in a horizontal pipe. J. Fluid Mech. 120, 385.

Yamamoto, Y., Potthoff, M., Tanaka, T., Kajishima, T., Tsuji, Y., 2001. Large eddy simulation of turbulent gas–solid flow in a vertical channel: effect of considering inter-particle collisions. J. Fluid Mech. 442, 303–334.

Yarin, L.P., Hetsroni, G., 1994. Turbulence intensity in dilute two-phase flow-3; the particles–turbulence interaction in dilute two-phase flow. Int. J. Multiphase Flow 20, 27–44.